Heliyon 10 (2024) e37061

Contents lists available at ScienceDirect

Heliyon

journal homepage: www.cell.com/heliyon

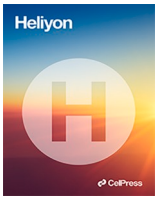

Research article

# Microscopic and macroscopic analysis of hexavalent chromium adsorption on polypyrrole-polyaniline@rice husk ash adsorbent using statistical physics modeling

Ismahene Ben Khemis [a,*], Fatma Aouaini [b], Salah Knani [c], Kholoud Saad Al-mugren [b], Abdelmottaleb Ben Lamine [a]

[a] Laboratory of Quantum and Statistical Physics LR 18 ES 18, Faculty of Sciences of Monastir, Environnement Street, 5019, Monastir, Tunisia
[b] Department of Physics, College of Science, Princess Nourah Bint Abdulrahman University, P.O. Box 84428, Riyadh, 11671, Saudi Arabia
[c] Department of Physics, College of Science, Northern Border University, Arar, Saudi Arabia

ARTICLE INFO

*Keywords:*
Polypyrrole-polyaniline@rice husk ash
Hexavalent chromium
Multi-layer model
Statistical physics theory
Physical modeling
Pore size distribution

ABSTRACT

This paper contributed with new findings to understand and characterize a heavy metal adsorption on a composite adsorbent. The synthesized polypyrrole–polyaniline@rice husk ash (PPY–PANI@RHA) was prepared and used as an adsorbent for the removal of hexavalent chromium Cr(VI). The adsorption isotherms of Cr(VI) ions on PPY–PANI@RHA were experimentally determined at pH 2, and at different adsorption temperatures (293, 303, and 313 K). Multi-layer model developed using statistical physics formalism was applied to theoretically analyze and characterize the different interactions and ion exchanges during the adsorption process for the elimination of this toxic metal from aqueous solutions, and to attribute new physicochemical interpretation of the process of adsorption. The physicochemical structures and properties of the synthesized PPY–PANI@RHA were characterized via Fourier transform infrared spectroscopy (FTIR). Fitting findings showed that the mechanism of adsorption of Cr(VI) on PPY–PANI@RHA was a multi-ionic mechanism, where one binding site may be occupied by one and two ions. It may also be noticed that the temperature augmentation generated the activation of more functional groups of the composite adsorbent, facilitating the interactions of metal ions with the binding sites and the access to smaller pore. The energetic characterization suggested that the mechanism of adsorption of the investigated systems was exothermic and Cr(VI) ions were physisorbed on PPY-PANI@RHA surface via electrostatic interaction, reduction of Cr(VI) to Cr (III), hydrogen bonding, and ion exchange. Overall, the utilization of the theory of statistical physics provided fruitful and profounder analysis of the adsorption mechanism. The estimation of the pore size distribution (PSD) of the polypyrrole-polyaniline@rice husk ash using the statistical physics approach was considered stereographic characterization of the adsorbent (here PPY–PANI@RHA was globally a meso-porous adsorbent). Lastly, the mechanism of Cr(VI) removal from wastewater using PPY-PANI@RHA as adsorbent was macroscopically investigated via the estimation of three thermodynamic functions.

* Corresponding author.
*E-mail address:* ismaheneph@gmail.com (I. Ben Khemis).

https://doi.org/10.1016/j.heliyon.2024.e37061
Received 16 April 2024; Received in revised form 15 June 2024; Accepted 27 August 2024
Available online 28 August 2024

## 1. Introduction

The potential harmful metal discharge from industries into the environment has generated public alarm with the increase of industrialization and population expansion because of its potentially dangerous impact on environmental security and human health [1–3]. Due to their high toxicity, persistence, and lack of biodegradability, potentially harmful metals are recognized as the main contaminant of the food chain since their accumulation in living tissues could lead to severe health and environmental hazards [4,5]. For example, chronic exposure to high levels of chromium may cause a number of ailments, including kidneys, and lungs, as well as causing adverse skin responses, vomiting, and severe diarrhea [6–8]. Chromium actually exists in a number of oxidation states, with Cr (III) and Cr(VI) being the most stable ones. In comparison to Cr(III), Cr(VI) is highly poisonous. It is more soluble, mutagenic, and carcinogenic [6]. According to a previous study by Beaumont et al. [9], a Chinese population exposed to Cr(VI) in drinking water has an elevated incidence of stomach cancer. These ions are mostly produced by the pesticide, paint, mining, tannery, and electroplating industries [10].

The remediation of wastewater containing potentially harmful metals has been carried out using a variety of physicochemical techniques [11–15]. However, these methods have certain drawbacks, including high energy needs, the production of hazardous sludge, and expensive costs [16]. Hence, the adsorption is one of the popular techniques used in treatment technologies to be an efficient technique for potentially harmful metal cleanup due to its simplicity of use, reduction of secondary waste, and cheap cost [17]. Indeed, several studies have been conducted on Cr(VI) ions removal from wastewater using bacteria cell templated porous polyaniline (maximum adsorbed quantity of 835.06 mg/g) [18], polypyrrole/calcium rectorite composites (maximum adsorbed quantity ranging from of 833.33 mg/g at 318 K) [19], PPy/$Fe_3O_4$ magnetic nanocomposites (maximum adsorbed quantity of 208.77 mg/g at 306 K) [20], capsular polypyrrole hollow nanofibers (maximum adsorbed quantity of 839.30 mg/g at 298 K) [21], core-shell $Fe_3O_4$/PANI microspheres (maximum adsorbed quantity of 200 mg/g at 298 K) [22], chitosan/polypyrrole (maximum adsorbed quantity of 92.16 mg/g at 323 K) [23], flake-like polyaniline/montmorillonite nanocomposites (maximum adsorbed quantity of 167.50 mg/g) [24], polyaniline@$Ni(OH)_2$ (maximum adsorbed quantity of 625 mg/g at 298 K) [25], $Fe_3O_4$@Arg-PPy (maximum adsorbed quantity of 322.58 mg/g at 298 K) [26], sodium alginate-polyaniline nanofibers (maximum adsorbed quantity of 73.34 mg/g at 303 K) [27], polypyrrole-modified layered double hydroxides (maximum adsorbed quantity of 76.21 mg/g at 298 K) [28], alkyl-substituted polyaniline/chitosan maximum adsorbed quantity of 2.66 mmol/g at 298 K) [29], graphene/$SiO_2$@polypyrrole (maximum adsorbed quantity of 429.18 mg/g at 298 K) [30], and PANI-coated electrospun adsorbent membranes (maximum adsorbed quantity of 15.08 mg/g at 298 K) [31]. It may then be remarked that different adsorbents have been successfully applied in removing chromium from aqueous solutions. Nearly all these studies have used models derived from the Langmuir theory, showing relatively low maximum adsorbed quantities. Regarding adsorption modeling, it may be noted that conventional models have been utilized to analyze adsorption equilibrium data. Nevertheless, the interpretations obtained from these models provide only a partial and incomplete comprehension of the adsorption process, in terms of equilibrium constant and maximum adsorption capacity.

The selection of polyaniline (PANI) and polypyrrole (PPY) for this study is primarily influenced by their easy bulk synthesis, redox properties, biocompatibility, non-toxic nature, substantial specific surface area, and affordability [20]. Additionally, the inclusion of a nitrogen atom with a lone pair of electrons in PPY and PANI enhances their capability for binding (hydrogen/electrostatic) within the macromolecular chains, thereby facilitating the effective removal of Cr(VI) ions from polluted water [18]. Nevertheless, post-treatment, the process of eluting PANI and PPY powder proves to be exceedingly laborious and costly, primarily due to its intrinsic hydrophilic nature. In this context, significant endeavors have been directed towards developing diverse PPY and PANI coatings on inexpensive, environmentally friendly bio-adsorbents such as rice husk ash (RHA), which is then utilized as adsorbent for the extraction of Cr(VI) ions from wastewater. As a result, the current study is centered on the creation of PPY-PANI composite coated on RHA and the investigation of its potential as an adsorbent for the elimination of Cr(VI) ions from wastewater. By using traditional models (Freundlich, Langmuir, Langmuir-Freundlich, and Temkin models), the adsorption of this contaminant has been well examined in terms of adsorption modeling [32,33]. Nevertheless, a number of investigations have revealed that the absence of quantitative analysis of physicochemical parameters prevents a complete description of the adsorption mechanism as interpreted by these models. The novelty of this work is associated with the characterization using FTIR analysis and the application of an advanced modeling study based on statistical physics approach. Hence, to deeper analyze and gain insights into the microscopic and the macroscopic levels of the adsorption mechanism, a multi-layer model has been established and used by examining its physicochemical parameters with clear physical significances in relation with the putative adsorption process [34–38].

In the current work, an advanced statistical physics model was carried out to study the Cr(VI) adsorption isotherms onto the polypyrrole-polyaniline@rice husk ash (PPY-PANI@RHA), at three temperatures (293, 303, and 313 K). Hence, the principal aim of this work was to quantitatively characterize the studied systems by highlighting and analyzing the significance of the estimated parameters.

## 2. Materials and methods

### 2.1. General

The stock solution of 1 g $L^{-1}$ of hexavalent chromium Cr(VI) was made by dissolving 2.82 g of potassium dichromate in 1 L of distillated water. The stock solution was successively diluted to produce the desired Cr(VI) concentrations.

The local rice mill provided the raw rice hush used in this work. The different chemicals and reagents, which were utilized in this work such as aniline monomers, pyrrole monomer, ammonium persulfate (APS), and potassium dichromate, were purchased from

Merck Pvt. Ltd. India. All chemicals were performed using double-distilled water.

The rice husks, which are a byproduct from the local rice mill, were washed multiple times with distilled water and were then dried in a hot air oven for 12 h at 333 K. Following this, the rice husks were pre-treated with 1 mol $L^{-1}$ of hydrochloric acid (HCl) before being combusted to generate pure white silica powder. Afterward, they were rinsed several times with deionized water to eliminate excess acid and subsequently dried in an oven for 24 h at 333 K. The resulting product was then heated in a muffle furnace for 4 h at 973 K, forming white rice husk ash (RHA) powder.

The synthesis of PPY–PANI@RHA was made according to the methods presented by Dutta et al. [33]. Firstly, 0.15 mL of aniline monomer, 0.3 mL of pyrrole monomer, and 10 mL of distilled water were mixed, doped with 1 M HCl and, and at the same time added to 0.1 g of RHA, which was dispersed in 10 mL of distilled water in a baker, at room temperature (303 K) for 5–6 h. Afterward, 0.15 g of APS dissolved in distilled water was added to the mixture, and the system was maintained in an ice bath for 12 h. The solid (i.e., PPY–PANI@RHA) was rapidly washed with distillated water multiple times, and then remained in a vacuum oven at 333 K for one day. The solid was recuperated by filtration, washed, and dried at 333 K, with subsequent calcinations at 973 K for 4 h using muffle furnace, for obtaining the PPY-PANI@RHA. Almost identical experimental methods were reported by previous works [39–48].

### 2.2. Adsorption isotherms

Firstly, solutions with a concentration of 1 g $L^{-1}$ of Cr(VI) were prepared by successive dilution of the stock solution until they reached the desired concentrations for the adsorption isotherm experiments.

The adsorption isotherms of the examined heavy metal were conducted at temperatures of 293, 303, and 313 K with initial concentrations of Cr(VI) of 0, 50, 100, 150, 200, 250, 300, 350, 400, 450, 500, 550, and 600 mg $L^{-1}$, contact time of 4 h, adsorbent dosage of 0.8 g $L^{-1}$, solution volume of 100 mL, pH 2, and stirring rate of 200 rpm.

Fig. 1 described the experimental hexavalent chromium adsorption isotherms on PPY–PANI@RHA at 293, 303, and 313 K and pH 2.

All experimental data showed that the adsorption temperature increased the adsorbed quantity of Cr(VI). Indeed, these experimental adsorption isotherms were fitted with an advanced model established using the statistical physics theory described below.

### 2.3. Statistical physics model

Several theoretical models, which were established in previous paper by Ben Lamine team [49–52], may be used for the adjustment of different types of isotherms with the aim of selecting the most appropriate model for each adsorption system. The adjustment of the experimental data through the use of the statistical physics theory may be considered potent method to microscopically and macroscopically investigate the adsorption of Cr(VI) ions from wastewater using PPY-PANI@RHA. Hence, in this work, the most general model with two adsorption energy levels (i.e., the multi-layer model) was chosen to study the mechanism of adsorption of hexavalent chromium [Cr(VI)] on PPY-PANI@RHA.

It was supposed that.

1) The adsorption of Cr(VI) occurred via the formation of infinity of layers.
2) The adsorbed heavy ions in the 1st layer acted as adsorbent for the 2nd and subsequent layers.
3) The Cr(VI) ions were adsorbed on the 1st layer with the adsorption energy ($-\varepsilon_1$) and on the $N_l$ layers with the adsorption energy ($-\varepsilon_2$).

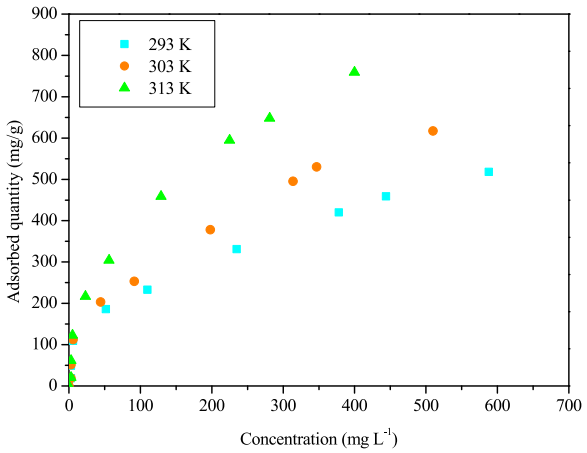


**Fig. 1.** Experimental isotherms of the adsorption isotherms of Cr(VI) ions on PPY-PANI@RHA at different temperatures (293, 303, and 313 K) and at pH 2 from aqueous solutions.

As proposed in previous paper [52], the theoretical expression of the adsorbed quantity $Q_a$ versus the adsorbate concentration at equilibrium $C$ may be written as:

$$Q_a = (nN_s)\times\left[\frac{-\left(\frac{2\left(\frac{C}{C_1}\right)^{2n}}{\left(1-\left(\frac{C}{C_1}\right)^{n}\right)}+\frac{\left(\frac{C}{C_1}\right)^{n}\left(1-\left(\frac{C}{C_1}\right)^{2n}\right)}{\left(1-\left(\frac{C}{C_1}\right)^{n}\right)^{2}}\right)+\left(\frac{2\left(\frac{C}{C_1}\right)^{n}\left(\frac{C}{C_2}\right)^{n}\left(1-\left(\frac{C}{C_2}\right)^{nN_l}\right)}{\left(1-\left(\frac{C}{C_2}\right)^{n}\right)}\right)+\left(-\frac{N_l\left(\frac{C}{C_1}\right)^{n}\left(\frac{C}{C_2}\right)^{n}\left(\frac{C}{C_2}\right)^{nN_l}}{\left(1-\left(\frac{C}{C_2}\right)^{n}\right)}\right)+\left(\frac{\left(\frac{C}{C_1}\right)^{n}\left(\frac{C}{C_2}\right)^{2n}\left(1-\left(\frac{C}{C_2}\right)^{nN_l}\right)}{\left(1-\left(\frac{C}{C_2}\right)^{n}\right)^{2}}\right)}{\left(\frac{\left(1-\left(\frac{C}{C_1}\right)^{2n}\right)}{\left(1-\left(\frac{C}{C_1}\right)^{n}\right)}\right)+\left(\frac{\left(\frac{C}{C_1}\right)^{n}\left(\frac{C}{C_2}\right)^{n}\left(1-\left(\frac{C}{C_2}\right)^{nN_l}\right)}{\left(1-\left(\frac{C}{C_2}\right)^{n}\right)}\right)}\right] \quad \text{(Eq. 1)}$$

In Eq. 1, $n$, $N_s$, $N_l$, $C_1$, and $C_2$ being five fitting parameters, which represented, respectively, the number of Cr(VI) ions docked on one binding site, the number of occupied PPY–PANI@RHA sites at saturation, the number of occupied layers, and the half-saturation concentrations.

The half-saturation concentration $C_i$ ($i = 1$ or 2) may be expressed as a function of the molar adsorption energy $\Delta E_i$ ($i = 1$ or 2) by the following expression [53]:

$$\Delta E_i = RT \ln\left(\frac{C_s}{C_i}\right) \quad \text{(Eq. 2)}$$

## 3. Results and discussion

### 3.1. Characterization of polypyrrole-polyaniline@rice husk ash

X-ray diffraction analysis (XRD) of RHA was conducted to determine the mineralogical phases (whether amorphous or crystalline). Indeed, Fig. 2 illustrated the XRD pattern of RHA sample comprising $SiO_2$ (89.50 %), $Fe_2O_3$ (2.86 %), CaO (0.30 %), $Al_2O_3$ (0.40 %), and other minor mineral element. The presence of a broad hump indicated its amorphous nature, while the peaks corresponding to $SiO_2$ suggested also its crystalline nature. It may then be deduced that RHA existed in both amorphous and crystalline forms. Notably, the prominent peak of crystalline $SiO_2$ is observed at 26° 2θ. The combustion of rice husks yields ash with a high silica content. When the combustion process of rice husks ash with high silica content was conducted under controlled conditions, the silica in RHA remained amorphous [33].

The surface functional groups of PPY–PANI@RHA and PPY–PANI@RHA-Cr(VI) were analyzed by FTIR analysis in the wavenumber range of 400–4000 $cm^{-1}$ and the corresponding spectra were illustrated in Fig. 3. The characteristic peaks of polyaniline in the spectra of PPY-PANI@RHA appeared at 1595, 1550, 1480, 1300, 1100, and 780 $cm^{-1}$, corresponding to C=N stretching, C-N stretching, C-C bonding of benzenoid structure, N-H deformation, -$NH^+$ = vibration in the structure, and C-Cl out-of plane, respectively [54,55]. In addition, the presence of the peaks at 1550 $cm^{-1}$ (C-N stretching), 1480 $cm^{-1}$ (C-N stretching), 1100 $cm^{-1}$ (C-N stretching vibration), 1050 $cm^{-1}$ (C-H stretching vibaration), 920 $cm^{-1}$ (N-H plane deformation), and 800 $cm^{-1}$ (deformation) could be attributed to the presence of dopped polypyrrole in PPY-PANI@RHA [56,57].

The bands located at 1300, 1100, and 320 $cm^{-1}$ majorly decreased in width and intensity thus showing the interactions of Cr(VI)

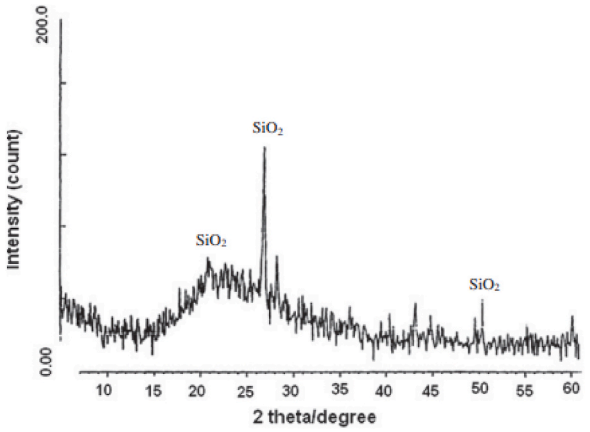


**Fig. 2.** XRD pattern of rice husk ash.

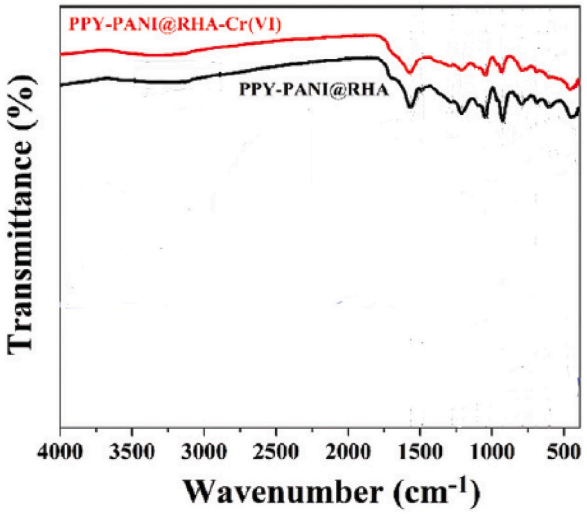


**Fig. 3.** FTIR spectra PPY-PANI@RHA before and after Cr(VI) adsorption.

with the main functional groups of in PPY-PANI@RHA, i.e., the two types of nitrogen-contained functional groups (N-H and -$NH^+$ = ).

### 3.2. Fitting results

In order to enhance the accuracy of predictions and deeply analyze the experimental isotherms, an advanced statistical physics model is used to adjust the experimental data set. This model aims to estimate various crucial parameters, including the number of heavy metal layers formed on PPY–PANI@RHA during the process of adsorption, the maximum adsorbed quantity of Cr(VI) ions, the density of functional groups, the number of layers, the half-saturation concentrations, and the associated adsorption energies.

The adjustment of the experimental hexavalent chromium adsorption isotherms on PPY-PANI@RHA at 293, 303, and 313 K and pH 2, depicted in Fig. 1, was achieved using the origin program (version 8.5). Based on the correlation coefficients ($R^2$) ranged from 0.99365 to 0.99624, the root mean square errors (*RMSE*) ranged from 0.02595 to 0.04698, and the physicochemical parameter values involved in the proposed model and their evolutions with temperature, it may be deduced that the multi-layer model offered a proper data fitting to characterize the nature and type of interactions occurred between the adsorbate and the adsorbent binding sites. This choice was made according to the generality of the used model since the multi-layer model was considered as the most general model with two adsorption energy levels, which may be used for any type of isotherm. These modeling results obtained by the application of the statistical physics theory were also supported by the adsorbent characterization using FTIR results, assuming that two main functional groups of PPY–PANI@RHA were involved in the adsorption of the studied heavy metal. Table 1 illustrated the modeling results and Fig. 4 presented the fitting of the experimental data using the multi-layer model.

The adsorption mechanism entailed an exchange of Cr(VI) ions from the free state to the adsorbed configuration. Hence, the utilization of the advanced and powerful statistical physics theory, specifically employing the grand canonical ensemble, becomes imperative to take into account the fluctuation in the number of heavy metal ions during the adsorption process. Indeed, this theoretical methodology may be applied to provide deeper analysis concerning the stereographic (saturation, orientation, aggregation degree, position, number of layers, density, adsorption manner, etc.) and energetic (adsorption energy, interaction type, adsorption type, adsorption nature, etc.) molecular interactions between the investigated adsorbate and the adsorbent binding sites. Unfortunately, the traditional models failed to provide relevant and quantitative insights into the adsorption phenomenon.

### 3.3. Analysis of the estimated parameters of the multi-layer model

The statistical physics theory established by Ben Lamine et al. [35–38,49–53] may be considered a potent and formidable method to profounder comprehend adsorption process involved in the removal of this water pollutant, analyze equilibrium data and provide

**Table 1**
Values of the correlation coefficient ($R^2$), and the residual root mean square error (*RMSE*) obtained from the adjustment of the adsorption isotherms of Cr (VI) ions by the multi-layer model.

| T (K) | $R^2$ | *RMSE* |
|---|---|---|
| **293** | 0.99624 | 0.02595 |
| **303** | 0.99365 | 0.04698 |
| **313** | 0.99566 | 0.03248 |

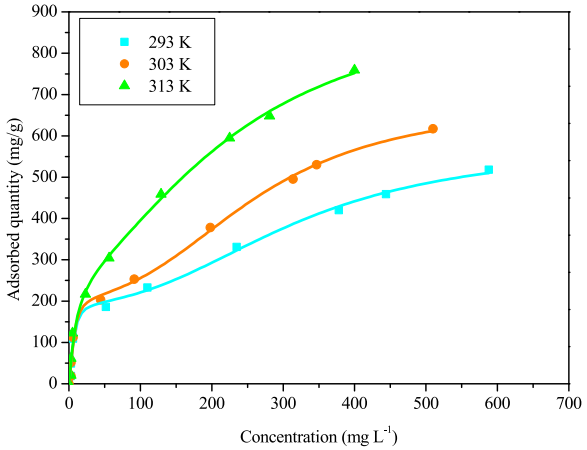


**Fig. 4.** Application of the multi-layer model on the adsorption isotherms of Cr(VI) ions on PPY-PANI@RHA at different temperatures (293, 303, and 313) and at pH 2.

physical explanations at a molecular level.

The adsorption mechanism of hexavalent chromium Cr(VI) may theoretically be investigated via stereographic and energetic parameters of the proposed model (i.e., the number of docked Cr(VI) ions per binding site $n$, the number of occupied adsorbent sites at saturation $N_S$, the total number of Cr(VI) layers $N_L$ ($N_L = N_l + 1$), the maximum adsorbed quantity $Q_M$, and the half-saturation concentrations $C_1$ and $C_2$). Notice that the molar adsorption energies $\Delta E_1$ and $\Delta E_2$ may be calculated via the estimated values of $C_1$ and $C_2$. Thus, all these physicochemical parameters are discussed with respect to solution temperature at a microscopic level in the next subheadings.

### *3.3.1. Number of docked Cr(VI) ions per binding site n*

In general, the first stereographic parameter $n$ may be applied to analyze and describe the chemical behavior of Cr(VI) ions during the adsorption process on PPY-PANI@RHA through the estimation of the aggregation degrees [49,51,58]. Indeed, the values of $n$ were superior to unity and ranged from 1.10 to 1.77. This fitting result suggested that Cr(VI) ions were aggregated but with a low degree.

Stereographically and geometrically, this estimated parameter may also provide profounder information concerning the position and the manner of binding of chromium ions on PPY–PANI@RHA surface during the process of adsorption. As mentioned above, all $n$ values were higher than unity ($1 < n < 2$) indicating the adsorbed Cr(VI) ions were linked as one or two ion(s) per PPY–PANI@RHA binding site. These stereographic findings suggested that the adsorption mechanism was multi-ionic and the adsorption geometry was non-parallel.

Table 2 presented the impact of the temperature on the number of docked chromium ions per binding site $n$. It may then be deduced that $n$ diminished as a function of adsorption temperature. Thus, this behavior may be attributed to the impact of thermal agitation, which may cause thermal collisions between hexavalent chromium ions leading to a reduction of the number of docked chromium ions per binding site, i.e., preventing the formed aggregate to be docked (thermal effect).

### *3.3.2. Number of occupied adsorbent sites at saturation $N_S$*

The number of occupied adsorbent binding sites at saturation $N_s$, second stereographic parameter, may present a great effect on the isotherm behavior.

Table 2 depicted the impact of the temperature on the number of occupied adsorbent sites at saturation $N_S$. It may be noticed that the temperature produced an increase of this parameter, i.e., an increment of the binding sites that are engaged in the Cr(VI) adsorption.

In addition, this density evolved with an inverse manner in comparison to the number of docked chromium ions per PPY–PANI@RHA binding site (i.e., when the values of the densities $N_S$ increased from 293 to 313 K, the corresponding values of $n$ decreased). Hence, the diminution of the number of docked chromium ions per binding site caused free space on PPY–PANI@RHA that generated the increase of $N_s$ since the formed aggregate decreased its size with the temperature (stereographic effect).

**Table 2**
Estimated parameters of multi-layer model for the adsorption of Cr(VI) ions on PPY–PANI@RHA.

| T (K) | $n$ | $N_S$ (mg/g) | $N_l$ | $N_L$ | $Q_M$ (mg/g) | $C_1$ (mg $L^{-1}$) | $C_2$ (mg $L^{-1}$) |
|---|---|---|---|---|---|---|---|
| **293** | 1.77 | 110.11 | 2.00 | 3.00 | 584.68 | 5.98 | 318.94 |
| **303** | 1.70 | 123.85 | 2.30 | 3.30 | 694.79 | 6.35 | 264.67 |
| **313** | 1.10 | 254.51 | 2.43 | 3.43 | 960.26 | 7.92 | 242.93 |

### 3.3.3. Total number of Cr(VI) layers $N_L$

The third stereographic parameter is the total number of Cr(VI) layers $N_L$ during the process of the adsorption that may be defined as [52]:

$$N_L = 1 + N_l \quad \text{(Eq. 3)}$$

The non-integer values of $N_L$ indicated that sometimes the layers were not fully occupied during the adsorption mechanism.

Table 2 depicted the effect of adsorption temperature on the number of formed layers of Cr(VI) on PPY–PANI@RHA during the adsorption process, which were varied from 3.00 to 3.43. It may then be deduced that up to four layers of hexavalent chromium were formed and $N_L$ augmented when the adsorption temperature augmented. This effect was presumably due to the increase of the interactions between the docked ions, i.e., Cr-Cr interactions.

### 3.3.4. Maximum adsorbed quantity at saturation $Q_M$

Lastly, the fourth stereographic parameter is the maximum adsorbed quantity. The expression of the maximum adsorbed quantity for a multi-layer model, which depended on the number of docked Cr(VI) ions per binding site $n$, the number of occupied adsorbent sites at saturation $N_S$, and the total number of Cr(VI) layers $N_L$, may be given by Ref. [52]:

$$Q_M = n \times N_S \times N_L \quad \text{(Eq. 4)}$$

It may be observed from Table 2 that the maximum adsorbed quantity at saturation increased with temperature (from 293 to 313 K), which may be explained by the augmentation in the mobility of the hexavalent chromium ions in aqueous solutions.

Finally, it was clear from the values of the different stereographic parameters introduced in the multi-layer model expression that the number of occupied adsorbent sites at saturation, the total number of Cr(VI) layers, and the maximum adsorbed quantity raised with temperature; however, the number of docked Cr(VI) ions per PPY–PANI@RHA binding site was reduced. The product of these three estimated parameters may mathematically explain the increment of the maximum adsorbed quantity with adsorption temperature.

### 3.3.5. Half-saturation concentrations $C_1$ and $C_2$

In the present study, the investigated adsorption systems were considered ideal systems since the different values of half-saturation concentrations $C_1$ and $C_2$, which were spread out from 5.98 to 9.92 mg $L^{-1}$, and from 242.93 to 318.94 mg $L^{-1}$, respectively, were not only far from the solubility concentration value ($C_s = 8.66\ 10^4$ mg $L^{-1}$) but also enough far from the saturation concentrations. As a result, interactions may be neglected for the investigated concentration intervals. Hence, $C_1$ and $C_2$ may be written as a function of the molar adsorption energies $\Delta E_1$ and $\Delta E_2$, respectively, as follows [46,49]:

$$\Delta E_1 = RT \ln\left(\frac{C_s}{C_1}\right) \quad \text{(Eq. 5)}$$

$$\Delta E_2 = RT \ln\left(\frac{C_s}{C_2}\right) \quad \text{(Eq. 6)}$$

these theoretical equations may be employed to calculate the molar adsorption energies $\Delta E_1$ and $\Delta E_2$ for the purpose of energetically interpreting the adsorption mechanism of one of the most frequent heavy metal contaminants presented in small quantities in natural waters. To simplify the energetic interpretation, the Cr(VI) solubility concentration in water was supposed to be invariant or constant at adsorption temperatures from 293 to 313 K and the estimated values of $C_1$ and $C_2$ were determined via the fitting of experimental isotherms at 293, 303 and 313 K.

Overall, it may be noted that $\Delta E_1$ described the interactions between Cr(VI) ions and PPY-PANI@RHA; however, $\Delta E_2$ described the Cr(VI)-Cr(VI) interactions. The removal of this toxic metal implied molar adsorption energy values ranging between 13.65 and 15.29 kJ/mol for the 1st layer and between 23.34 and 24.20 kJ/mol for the other layers (Table 3). Hence, all the estimated values of $\Delta E_1$ and $\Delta E_2$ were relatively low and inferior to 24 kJ/mol. Consequently, the adsorption of Cr(VI) on PPY-PANI@RHA was related to a physisorption process. It may also be observed that the positive values of the adsorption energies showed that the adsorption of this heavy metal was exothermic [49]. The interaction mechanism might include hydrogen bonding, electrostatic interaction, reduction and ion exchange. Indeed, the most prominent form of Cr(VI) was changeable versus the pH of the solution and at pH 2, as was the case in the this study, the most prominent form was $HCrO_4^-$ [19,33,59,60]. Note that a strong repulsive electrostatic interactions between Cr (VI) ions and PPY-PANI@RHA surface were occurred when pH (solution) > $pH_{pzc}$ (adsorbent). However, an attractive electrostatic interactions occurred when pH (solution) < $pH_{pzc}$ (adsorbent) since the $pH_{pzc}$ (PPY–PANI@RHA) was equal to 10.1, thus the Cr(VI)

**Table 3**
Estimated molar adsorption energies for the adsorption of Cr(VI) on PPY–PANI@RHA.

| T (K) | $C_1$ (mg $L^{-1}$) | $C_2$ (mg $L^{-1}$) | $\Delta E_1$ (kJ/mol) | $\Delta E_2$ (kJ/mol) |
|---|---|---|---|---|
| **293** | 5.98 | 318.94 | 23.34 | 13.65 |
| **303** | 6.35 | 264.67 | 23.98 | 14.58 |
| **313** | 9.92 | 242.93 | 24.20 | 15.29 |

ions were electrostatically anchored by positively charged amine functional groups (-NH-, -N<, -$NH_2$). Hydrogen bonding can then be considered after the interaction between hydrogen atoms in $HCrO_4^-$ ions and oxygen containing groups of the carboxylic functional groups. Furthermore, in an acidic environment, Cr(VI) can undergo reduction to Cr(III) due to its elevated redox potential [33] since hexavalent chromium species exhibited significant pH dependency. At lower pH levels, the surface functional groups of PANI@RHA became protonated, acquiring positive charges (–$NH^+$). This protonation favored electrostatic interactions with the primary anionic form of hexavalent chromium $HCrO_4^-$. Additionally, these functional groups served as electron donors, facilitating the reduction of Cr (VI) to Cr(III) with reduced toxicity [34]. Finally, it may also be deduced ion exchange between doped $Cl^-$ ions present on PPY-PANI@RHA surface with the $HCrO4^-$ ions.

Table 3 showed the impact of the adsorption temperature on the molar adsorption energy. It was clear that the values of the molar adsorptions increased with adsorption temperatures (from 293 to 313 K). This behavior may be explained by the raise of binding sites.

### 3.3.6. *Effect of experimental conditions on the adsorption of Cr(VI)*

The initial pH of the solution significantly influences the adsorption of chromium species by controlling the surface charges of the adsorbent. Fig. 5a illustrated the variation of % removal of Cr(VI) versus the initial pH at 313 K and at a fixed concentration (800 mg $L^{-1}$) of PPY–PANI@RHA. It is apparent that the adsorption behavior of Cr(VI) was strongly influenced by the pH. In this figure, it may be seen that the removal efficiency of Cr(VI) drastically declined from 99.87 % to 19.88 % as pH values transition from 2 to 12. Consequently, all subsequent adsorption experiments were conducted at pH 2 to ensure maximal Cr(VI) removal by PPY–PANI@RHA. In addition, it may be noted that Cr(VI) existed in various stable forms, such as $HCrO_4^-$, $Cr2O_7^{2-}$, and $CrO_4^{2-}$ in aqueous solutions depending on the chromium concentration and the pH of the solution. Typically, at pH levels between 1 and 5, $HCrO4^-$ prevails as the most dominant form. As pH increased, $HCrO_4^-$ was rapidly converted to $CrO_4^{2-}$. It may also deduced from these findings that the maximum rate of Cr(VI) removal of 99.87 % from the aqueous solution was observed at an optimal pH of 2, showing high ion-exchange between $HCrO4^-$ ions in the Cr(VI) solution and doped $Cl^-$ ions on the surface of the adsorbent [60]. Furthermore, at low pH, the adsorbent surface was highly protonated (i.e., positively charged), this led to electrostatic attraction between the negative charged chromium ions and the positively charged PPY–PANI@RHA binding sites. Additionally, it may be noticed that the reduction of Cr(VI)

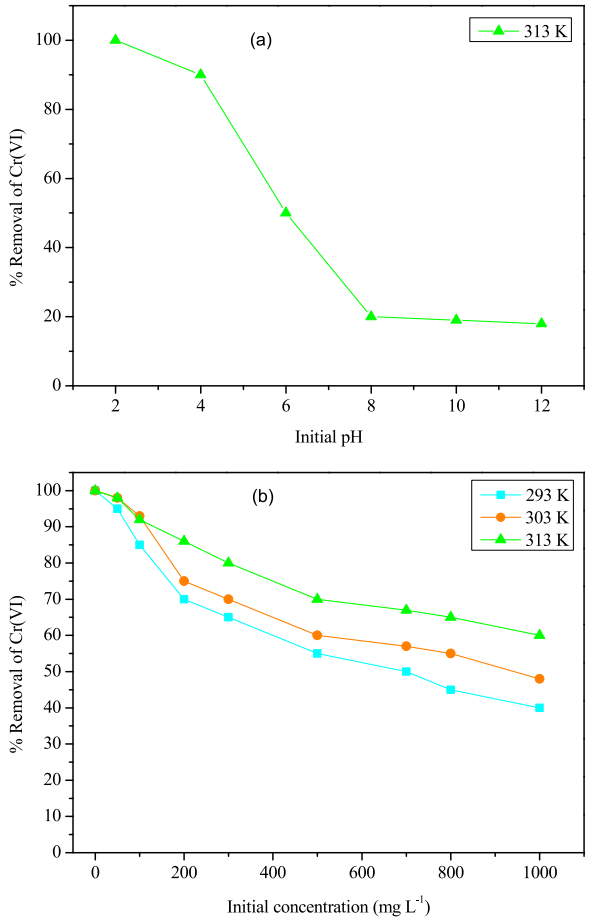


**Fig. 5.** Effect of (a) initial solution pH on % removal of Cr(VI) (Initial Cr(VI) concentration: 50 mg $L^{-1}$; temperature: 303 K), (b) initial concentration of Cr(VI) at a different temperature (pH 2).

to Cr(III) was also favored at low pH.

Fig. 5b depicted the % removal of Cr(VI) versus the initial concentration (10–1000 mg $L^{-1}$) at pH 2 and at three distinct temperatures (293, 303, and 313 K). It may be observed from this figure that the % removal of Cr(VI) decreased with increasing chromium concentration at all three temperatures. Specifically, the % removal of Cr(VI) decreased from 99.76 % to 40.12 %, from 99.85 % to 49.04 %, and from 99.91 % to 60.71 % corresponding to initial Cr(VI) concentrations from 10 to 1000 mg $L^{-1}$ at 293, 303, and 313 K, respectively. Additionally, these findings showed an increase in % removal of Cr(VI) with rising temperature, suggesting the exothermic nature of Cr(VI) adsorption on PPY-PANI@RHA. Thus, at all initial concentrations, it may be deduced that the maximum removal of Cr(VI) can be attributed to the heightened thermal energy of the docked chromium forms with increasing temperature [60].

### 3.3.7. Comparison of the adsorption capacity of PPY-PANI@RHA with literature report

Numerous adsorption materials have been reported for the effective removal of Cr(VI) from wastewater. These included sepiolite-supportes magnetite nanoparticles (SSMNPs), $Fe_2O_3$-chitosan-cherry kernel shell pyrolytic charcoal composite, Magnetic pinecone beads Poly (methyl methacrylate) + grafted alginate/$Fe_3O_4$ nanocomposite, Graphene oxide functionalized chitosan-magnetite nanocomposite, fibrous silica nanospheres KCC-1, $NH_2$-functionalized nano-sized magnetic metal–organic frameworks (MOFs), and carbonized zeolite/Chitosan composite as an adsorbent for copper (II) and chromium (VI) removal from water [61–63].

The maximum adsorbed quantities at saturation of PPY-PANI@RHA for Cr(VI) removal were then compared with those obtained in previous studies using the above adsorbents (Table 4). Hence, it may be noted from Table 4 that PPY-PANI@RHA showed high adsorption performance compared to the other adsorbents indicating that PPY-PANI@RHA demonstrated a very good adsorption capacity toward Cr(VI) ions.

## 3.4. Surface stereographic characterization

The stereographic characterization of porous adsorbents as PPY–PANI@RHA, the calculation of the pore size distribution (PSD) using the multi-layer model expression was fundamental, which was applied to estimate the pore densities versus the radius of pores [49,52,66]. According to Dutta et al. [33], the PSD of PPY–PANI@RHA presented a very large number of pores in the size range of 2–5 nm. For the calculation of the different PSDs, the Kelvin equation and the selected statistical physics model [49,52,67–71] were utilized as:

$$\frac{C}{C_s} = e^{-\frac{C_K}{r}} \quad \text{(Eq. 7)}$$

$C_K$ is the Kelvin constant (nm).

$r$ is the pore radius (nm)

Since

$$C_1 = C_s e^{\frac{\Delta E_1}{RT}} \quad \text{(Eq. 8)}$$

The adsorbed quantity expression may be written as a function of pore radius $r$ and Kelvin constant $C_k$ by substituting the relation $\frac{C_1}{C} = e^{\frac{C_K}{r}} e^{-\frac{\Delta E_1}{RT}}$ in the multi-layer model expression (i.e., introduction of the Kelvin equation into the proposed statistical physics model).

The PSD expression may then be calculated as the derivative of the adsorbed quantity equation relative to PPY–PANI@RHA pore radius [52,66]:

$$PSD = \frac{dQ_a}{dr} \quad \text{(Eq. 9)}$$

From Fig. 6, it may be noted that the pore sizes varied between 1 and 30 nm for the investigated adsorbent at different adsorption temperatures (293, 303, and 313 K), this findings affirmed that PPY–PANI@RHA adsorbent was a mesoporous material and presented heterogeneous surface since a large amount of pores were in the size range of 2.50–5.50 nm. The average values of radius observed from the peak the maximums were 4.42 nm, 4.27 nm, and 2.80 nm for PPY–PANI@RHA at 293, 303, and 313 K, respectively. These average pore radius measurements were consistent with the earlier findings as was expected [33]. Furthermore, it may be noticed from Fig. 6 that the PSDs shifted towards the low pore sizes with the increase of the adsorption temperature, since an increment in

**Table 4**
Adsorbed quantities at saturation of other adsorbents for Cr(VI).

| Adsorbents | $Q_M$ (mg/g) | Conditions | References |
|---|---|---|---|
| Sepiolite-supportes magnetite nanoparticles (SSMNPs) | 33.4 | pH 3, 293 K | [64] |
| $Fe_2O_3$-chitosan-cherry kernel shell pyrolytic charcoal composit | 47.58 | pH 2, 298 K | [65] |
| Magnetic pinecone beads Poly (methyl methacrylate)- grafted alginate/$Fe_3O_4$ nanocomposite | 132.52 | pH 2, 293 K | [34] |
| Graphene oxide functionalized chitosan-magnetite nanocomposite | 142.85 | pH 3, 303 K | [32] |
| Polypyrrole-polyaniline@rice husk ash (PPY–PANI@RHA) | 584.68 | pH 2, 293 K | This study |
| | 694.79 | pH 2, 303 K | |
| | 960.26 | pH 2, 313 K | |

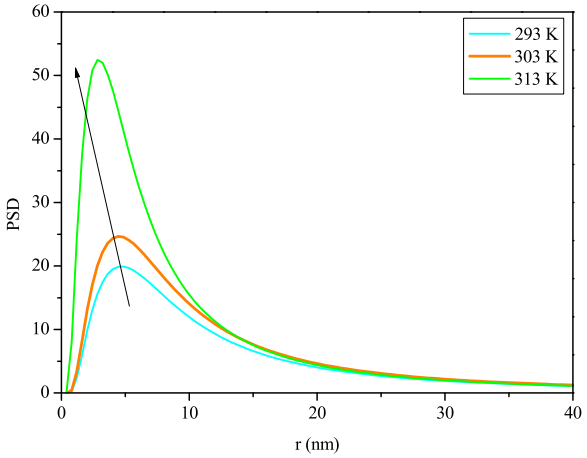


**Fig. 6.** Pore size distributions of PPY-PANI@RHA at different temperatures (293, 303, and 313) and at pH 2.

temperature leaded to an enhancement of the thermal excitation, which allowed the chromium ions to more easily enter small pores where there were fewer collisions. It may then deduce that the temperature augmentation yielded more available functional groups of PPY–PANI@RHA, which facilitated the access to smaller pores.

## 4. Thermodynamic investigation

Using the advanced multi-layer model, the internal energy, the Gibbs free energy, and the adsorption entropy may be determined and investigated. Thus, a detailed analysis of these functions, which macroscopically described the adsorption mechanism of Cr(VI) on PPY-PANI@RHA, was made in the following paragraphs.

The first thermodynamic function is the internal energy $E_{int}$, which may be considered the total energy due to the interactions between Cr(VI) ions and PPY-PANI@RHA surface. Thus, the theoretical expression of $E_{int}$ using the statistical physics theory may be given by Refs. [49,72]:

$$E_{\text{int}} = -\frac{\partial \ln Z_{gc}}{\partial \beta} + \frac{\mu}{\beta}\left(\frac{\partial \ln Z_{gc}}{\partial \mu}\right) \quad \text{(Eq. 10)}$$

Fig. 7a presented the behavior of $E_{int}$ versus Cr(VI) concentration for the three adsorption temperatures (293, 303, and 313 K). Thus, it can be remarked from this figure that the values of the macroscopic internal energy were negative, which allowed to deduce that the adsorption system (Cr(VI) + PPY-PANI@RHA) released energy to aqueous solutions to be adsorbed for the three temperatures. This behavior confirmed the exothermic nature of the studied process [38]. In addition, $E_{int}$ decreased algebraically from 0 with the increase of Cr(VI) concentration since a large number of PPY-PANI@RHA binding pores or sites were vacant at the beginning of the mechanism of adsorption.

The study of the impact of the adsorption temperature showed that $E_{int}$ decreased algebraically (increased in module) with the increase of temperature, which may be explained by the fact that the adsorption system evolved towards a more stable state. It may then be deduced that the system presented a tendency to decrease its internal energy.

The Gibbs free energy $G$ may be used to characterize the spontaneity of the three adsorption systems considered open systems. Hence, the theoretical expression of $G$ using the statistical physics theory can be given by Refs. [49,72]:

$$G = \mu Q_a \quad \text{(Eq. 11)}$$

Fig. 7b depicted the behavior of $G$ versus Cr(VI) concentration for three adsorption temperatures (293, 303, and 313 K). It may be noticed from this figure that the values of $G$ are always negative and the mechanism of adsorption of Cr(VI) ions on PPY-PANI@RHA is spontaneous [38,52]. It may also remark that the adsorption of this metal was more favorable at low concentrations.

The study of the impact of the adsorption temperature indicated that the increase of temperature from 293 to 313 K deceased algebraically the investigated system (Cr(VI) + PPY-PANI@RHA) spontaneity.

The third thermodynamic function is the adsorption entropy $S_a$, which may be used to describe the order and disorder and to characterize the behavior of the adsorption of Cr(VI) ions on PPY-PANI@RHA surface during the mechanism. Hence, the theoretical expression of $S_a$ can be defined on the basis of the grand canonical partition function $Z_{gc}$ in statistical physics as follows [49,72]:

$$\frac{S_a}{k_B} = -\beta\frac{\partial \ln Z_{gc}}{\partial \beta} + \ln Z_{gc} \quad \text{(Eq. 12)}$$

Fig. 7c illustrated the behavior of $S_a$ versus Cr(VI) concentration for the three adsorption temperatures (293, 303, and 313 K). According to this figure, it may be seen that the three entropy curves presented similar shapes before and after the half-saturation

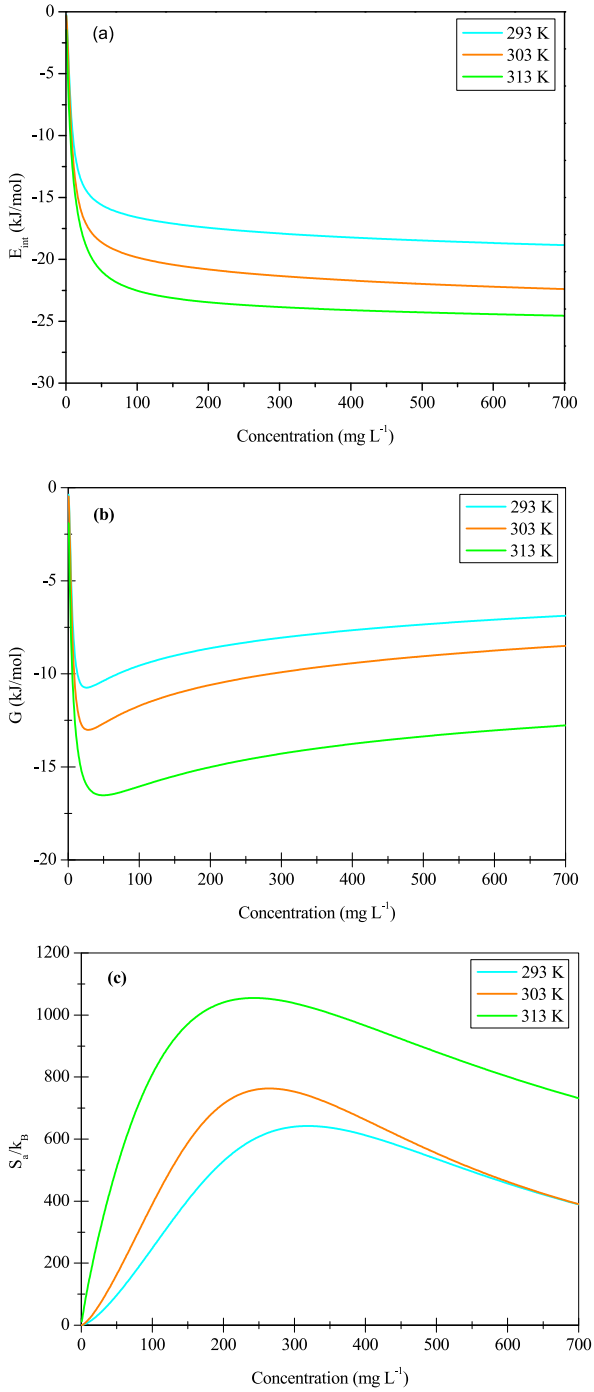


**Fig. 7.** Evolution of the internal energy (a), the Gibbs free energy (b), and the adsorption entropy (c) as a function of Cr(VI) concentration for the multi-layer adsorption on PPY-PANI@RHA

concentrations. For $C < C_1$, the Cr(VI) ions presented several possibilities to find empty PPY-PANI@RHA sites to be docked. It may then be deduced that the disorder of Cr(VI) ions on PPY-PANI@RHA surface increased until reaching a first maximum at $C_1$. For $C > C_1$, the metal ions had low probabilities to find vacant PPY-PANI@RHA sites. So, the disorder decreased since PPY-PANI@RHA surface tended toward first layer saturation. Thus, the obtained minimum did not reach 0 since the $N_l$ layers started to be occupied. As second step, the disorder increased again, but the first layer was now used as adsorbent for the $N_l$ layers. The same behaviors of $S_a$ were observed below and after the second maximum at $C_2$. In the present case, the first maximum is hidden since $C_1$ value was negligible compared to $C_2$ value). At the end of the adsorption mechanism (saturation phenomenon), the disorder diminished and may reach 0 since PPY-

PANI@RHA surface tends towards order.

The study of the impact of the adsorption temperature showed that for a fixed concentration the adsorption entropy (disorder) increased with the increment of the temperature due to the thermal agitation.

## 5. Conclusion

In conclusion, the adsorption process of Cr(VI) ions on a synthesized PPY–PANI@RHA was determined at three adsorption temperatures (293, 303, and 313 K). Under experimental conditions, the isotherms were well fitted using a multi-layer model, which provided new microscopic and macroscopic analysis of the studied systems during the adsorption mechanism. The mechanism of adsorption was investigated by FTIR analysis and the obtained results supported modeling findings. Stereographically speaking, fitting results indicated that the adsorbed quantity of Cr(VI) and the maximum adsorbed quantity increased with the increment of the adsorption temperature. The number of ions per one PPY–PANI@RHA binding site suggested that each site may be occupied by one and two metal ions via a multi-ionic mechanism where the high temperatures decreased this physicochemical parameter without affecting the anchorage manner on the studied adsorbent. Energetically speaking, the removal of this toxic metal implied molar adsorption energy values ranging between 13.65 and 15.29 kJ/mol for the 1st layer, and between 23.34 and 24.20 kJ/mol for the other layers, showing physical adsorption type (energy values lower than 25 kJ/mol) and exothermic adsorption nature (positive energy values). Thus, it may then be noted that the investigated process occurred via physical interactions like hydrogen bonding, electrostatic interaction, reduction, and ion exchange. The calculation of polypyrrole-polyaniline@rice husk ash PSDs using the statistical physics approach was considered direct and physical characterization of the adsorbent (here PPY-PANI@RHA was globally a meso-porous adsorbent). The three adsorption systems may also be studied at a macroscopic level through the investigation of three thermodynamic parameters, showing that the mechanism of adsorption evolved spontaneously with an exothermic character until the saturation state and the disorder maximum was observed at half saturation concentrations.

## Funding

The authors express their gratitude to Princess Nourah bint Abdulrahman University Researchers Supporting Project (Grant No. PNURSP2024R10), Princess Nourah bint Abdulrahman University, Riyadh, Saudi Arabia.The authors extend their appreciation to the Deanship of Scientific Research at Northern Border University, Arar, KSA for funding this research work through the project number "NBU-FFR-2024-2483-07"

## Ethics approval

Not applicable.

## Consent to participate

Not applicable.

## Consent for publication

Not applicable.

## CRediT authorship contribution statement

**Ismahene Ben Khemis:** Writing – original draft, Software, Project administration, Methodology, Investigation, Formal analysis, Conceptualization, Writing – review & editing, Funding acquisition. **Fatma Aouaini:** Formal analysis, Conceptualization, Supervision. **Salah Knani:** Conceptualization, Funding acquisition, Methodology, Software, Writing – original draft. **Kholoud Saad Al-mugren:** Conceptualization. **Abdelmottaleb Ben Lamine:** Writing – original draft.

## Declaration of competing interest

The authors declare that there are no conflicts of interest regarding the research contained in the paper.

## References

[1] M. Jain, M. Yadav, T. Kohout, M. Lahtinen, V.K. Garg, M.J.W.r. Sillanpää, Development of iron oxide/activated carbon nanoparticle composite for the removal of Cr (VI), Cu (II) and Cd (II) ions from aqueous solution, Water Resour. Ind. 20 (2018) 54–74.

[2] A.Q. Selim, L. Sellaoui, S.A. Ahmed, M. Mobarak, E.A. Mohamed, A. Ben Lamine, A. Erto, A. Bonilla-Petriciolet, M.K. Seliem, Statistical physics-based analysis of the adsorption of Cu2+ and Zn2+ onto synthetic cancrinite in single-compound and binary systems, J. Environ. Chem. Eng. 7 (2019) 103217.

[3] F. Zhang, X. Tang, Y. Huang, A.A. Keller, J. Lan, Competitive removal of Pb2+ and malachite green from water by magnetic phosphate nanocomposites, Water Res. 150 (2019) 442–451.

[4] W.W. Ngah, M.M.J.B.t. Hanafiah, Removal of heavy metal ions from wastewater by chemically modified plant wastes as adsorbents: a review, Bioresour. Technol. 99 (2008) 3935–3948.
[5] C. Barquilha, E. Cossich, C. Tavares, E. Silva, Biosorption of nickel (II) and copper (II) ions by Sargassum sp. in nature and alginate extraction products, Bioresour. Technol. Rep. 5 (2019) 43–50.
[6] A. Zhitkovich, Chromium in drinking water: sources, metabolism, and cancer risks, Chem. Res. Toxicol. 24 (2011) 1617–1629.
[7] I. Aharchaou, J.S. Py, S. Cambier, J.L. Loizeau, G. Cornelis, P. Rousselle, E. Battaglia, D.A. Vignati, Chromium hazard and risk assessment: new insights from a detailed speciation study in a standard test medium, Environ. Toxicol. Chem. 37 (2018) 983–992.
[8] B. Chen, J. Xiong, J.-H. Ding, B.-F. Yuan, Y.-Q. Feng, Analysis of the effects of Cr (VI) exposure on mRNA modifications, Chem. Res. Toxicol. 32 (2019) 2078–2085.
[9] J.J. Beaumont, R.M. Sedman, S.D. Reynolds, C.D. Sherman, L.-H. Li, R.A. Howd, M.S. Sandy, L. Zeise, G.V. Alexeeff, Cancer mortality in a Chinese population exposed to hexavalent chromium in drinking water, Epidemiology (2008) 12–23.
[10] J. Barnhart, Occurrences, uses, and properties of chromium, Regul. Toxicol. Pharmacol. 26 (1997) S3–S7.
[11] Y. Al-Degs, M. Khraisheh, M. Tutunji, Sorption of lead ions on diatomite and manganese oxides modified diatomite, Water Res. 35 (2001) 3724–3728.
[12] N. Chitpong, S.M. Husson, High-capacity, nanofiber-based ion-exchange membranes for the selective recovery of heavy metals from impaired waters, Separation and Purification Technology 179 (2017) 94–103.
[13] N. Meunier, P. Drogui, C. Montané, R. Hausler, G. Mercier, J.-F. Blais, Comparison between electrocoagulation and chemical precipitation for metals removal from acidic soil leachate, J. Hazard Mater. 137 (2006) 581–590.
[14] S. Mukherjee, S. Mukhopadhyay, A. Pariatamby, M.A. Hashim, G. Redzwan, B.S. Gupta, Optimization of pulp fibre removal by flotation using colloidal gas aphrons generated from a natural surfactant, J. Taiwan Inst. Chem. Eng. 53 (2015) 15–21.
[15] K. Yan, Z. Liu, Z. Li, R. Yue, F. Guo, Z. Xu, Selective separation of chromium from sulphuric acid leaching solutions of mixed electroplating sludge using phosphate precipitation, Hydrometallurgy 186 (2019) 42–49.
[16] H.E. Reynel-Avila, D.I. Mendoza-Castillo, V. Hernández-Montoya, A. Bonilla Petriciolet, Multicomponent Removal of Heavy Metals from Aqueous Solution Using Low-Cost Sorbents, Nova Science Publisher, New York, 2011, pp. 69–99.
[17] I. Ali, New generation adsorbents for water treatment, Chem. Rev. 112 (2012) 5073–5091.
[18] K. Gong, S. Guo, Y. Zhao, Q. Hu, H. Liu, D. Sun, M. Li, B. Qiu, Z. Guo, Bacteria cell templated porous polyaniline facilitated detoxification and recovery of hexavalent chromium, J. Mater. Chem. A 6 (2018) 16824–16832.
[19] Y. Xu, J. Chen, R. Chen, P. Yu, S. Guo, X. Wang, Adsorption and reduction of chromium(VI) from aqueous solution using polypyrrole/calcium rectorite composite adsorbent, Water Res. 160 (2019) 148–157.
[20] U.O. Aigbe, R. Das, W.H. Ho, V. Srinivasu, A. Maity, A novel method for removal of Cr(VI) using polypyrrole magnetic nanocomposite in the presence of unsteady magnetic fields, Separation and Purification Technology 194 (2018) 377–387.
[21] J. Zhao, Z. Li, J. Wang, Q. Li, X. Wang, Capsular polypyrrole hollow nanofibers: an efficient recyclable adsorbent for hexavalent chromium removal, J. Mater. Chem. A 3 (2015) 15124–15132.
[22] X. Han, L. Gai, H. Jiang, L. Zhao, H. Liu, dan W. Zhang, Core–shell structured Fe3O4/PANI microspheres and their Cr(VI) ion removal properties, Synth. Met. 171 (2013) 1–6.
[23] R. Karthik, S. Meenakshi, Removal of hexavalent chromium ions from aqueous solution using chitosan/polypyrrole composite, Desalination Water Treat. 56 (2015) 1587–1600.
[24] J. Chen, X. Hong, Y. Zhao, Y. Xia, D. Li, Q. Zhang, Preparation of flake-like polyaniline/montmorillonite nanocomposites and their application for removal of Cr (VI) ions in aqueous solution, J. Mater. Sci. 48 (2013) 7708–7717.
[25] M. Bhaumik, V.K. Gupta, A. Maity, Synergetic enhancement of Cr(VI) removal from aqueous solutions using polyaniline@$Ni(OH)_2$ nanocomposites adsorbent, J. Environ. Chem. Eng. 6 (2018) 2514–2527.
[26] M. Chigondo, H.K. Paumo, M. Bhaumik, K. Pillay, A. Maity, Magnetic arginine-functionalized polypyrrole with improved and selective chromium (VI) ions removal from water, J. Mol. Liq. 275 (2019) 778–791.
[27] R. Karthik, S. Meenakshi, Removal of Cr(VI) ions by adsorption onto sodium alginate-polyaniline nanofibers, Int. J. Biol. Macromol. 72 (2015) 711–717.
[28] S. Sahu, P. Kar, N. Bishoyi, N.L. Mallik, R.K. Patel, Synthesis of polypyrrole-modified layered double hydroxides for efficient removal of Cr(VI), J. Chem. Eng. Data 64 (2019) 4357–4368.
[29] A.G. Yavuz, E. Dincturk-Atalay, A. Uygun, F. Gode, E. Aslan, A comparison study of adsorption of Cr(VI) from aqueous solutions onto AlkylSubstituted polyaniline/chitosan composites, Desalination 279 (2011) 325–331.
[30] W. Fang, X. Jiang, H. Luo, J. Geng, Synthesis of graphene/SiO2@polypyrrole nanocomposites and their application for Cr(VI) removal in aqueous solution, Chemosphere 197 (2018) 594–602.
[31] G. Dognani, P. Hadi, H. Ma, F.C. Cabrera, A.E. Job, D.L.S. Agostini, B.S. Hsiao, Effective chromium removal from water by polyaniline-coated electrospun adsorbent membrane, Chem. Eng. J. 372 (2019) 341–351.
[32] S. Anush, H. Chandan, B. Gayathri, N. Manju, B. Vishalakshi, B. Kalluraya, Graphene oxide functionalized chitosan-magnetite nanocomposite for removal of Cu (II) and Cr (VI) from waste water, Int. J. Biol. Macromol. 164 (2020) 4391–4402.
[33] S. Dutta, S.K. Srivastava, A.K. Gupta, Polypyrrole–polyaniline copolymer coated green rice husk ash as an effective adsorbent for the removal of hexavalent chromium from contaminated water, Royal Society of Chemistry 2 (2021) 2431.
[34] M. Touihri, F. Guesmi, C. Hannachi, B. Hamrouni, L. Sellaoui, M. Badawi, J. Poch, N. Fiol, Single and simultaneous adsorption of Cr(VI) and Cu (II) on a novel Fe3O4/pine cones gel beads nanocomposite: experiments, characterization and isotherms modeling, Chem. Eng. J. 416 (2021) 129101.
[35] K. Oueslati, A. Naifa, G.Z. Kyzas, A. Ben Lamine, Thermodynamic interpretation of cationic dye adsorption onto untreated coffee residues as adsorbents via statistical physics approach, J. Mol. Struct. 1311 (2024) 138387.
[36] X. Diao, L. Zhang, Q. Li, X. Gao, M.K. Seliem, F. Dhaoudi, L. Sellaoui, S. Deng, A. Bonilla-Petriciolet, M. Badawi, Z. Li, Adsorption of food dyes from aqueous solution on a sweet potato residue-derived carbonaceous adsorbent: analytical interpretation of adsorption mechanisms via adsorbent characterization and statistical physics modeling, Chem. Eng. J. 482 (2024) 148982.
[37] L. Sellaoui, F. Edi-Soetaredjo, M. Mbarek, S. Ismadji, B. Ernst, A. Bonilla-Petriciolet, A. Ben Lamine, D. Dell'Angelo, M. Badawi, A novel application of HKUST-1 for textile dyes removal in single and binary solutions: experimental investigation combined with physical modelling, Chem. Eng. J. 480 (2024) 147958.
[38] A. Atri, F. Dhaoudi, N. Mechi, L. Sellaoui, M. Echabaane, R. Ben Chaabene, A. Erto, M. Badawi, A. Ben Lamine, Removal of textile pollutants from aqueous medium using biosynthesized CuO nanoparticles: theoretical comparative investigation via analytical model, Helyion 10 (2024) e26285.
[39] G.L. Dotto, J. Vieillard, D. Pinto, S.F. Lütke, L.F.O. Silva, G. Dos Reis, É.C. Lima, S.P.F. Dison, Selective adsorption of gadolinium from real leachate using a natural bentonite clay, J. Environ. Chem. Eng. 11 (2023) 109748.
[40] R.B.H.B. Farias, D. Pinto, M.L. Goulart, A.V. Igansi, L. Loebens, M. Y'lmaz, L.F.O. Silva, R. Andreazza, T.R.S. Cadaval, M.S. Quadro, Treatment of residual lubricating oil using rice husk-based material as ecological adsorbent, J. Mater. Cycles Waste Manag. 25 (2023) 52–61.
[41] B.D. Lima, E.C. Teixeira, J.C. Hower, M.S. Civeira, O. Ramírez, C. Yang, M.L.S. Oliveira, L.F.O. Silva, Metal-enriched nanoparticles and black carbon: a perspective from the Brazil railway system air pollution, Geosci. Front. 12 (2021) 101129.
[42] V.X. Nascimento, C. Schnorr, S.F. Lütke, M.C.F. Da Silva, F. Machado Machado, P.S. Thue, É.C. Lima, J. Vieillard, L.F.O. Silva, G.L. Dotto, Adsorptive features of magnetic activated carbons prepared by a one-step process towards brilliant blue dye, Molecules 28 (2023) 1821.
[43] M.L.S. Oliveira, E.M.M. Flores, G.L. Dotto, A. Neckel, L.F.O. Silva, Nanomineralogy of mortars and ceramics from the Forum of Caesar and Nerva (Rome, Italy): the protagonist of black crusts produced on historic buildings, J. Clean. Prod. 278 (2021) 123982.
[44] H.A. Pereira, K. Da Boit Martinello, Y. Vieira, J.C. Diel, M.S. Netto, G.D. Reske, E. Lorenzett, L.F.O. Silva, T.A.L. Burgo, G.L. Dotto, Adsorptive behavior of multi-walled carbon nanotubes immobilized magnetic nanoparticles for removing selected pesticides from aqueous matrices, Chemosphere 325 (2023) 138384.

[45] R.K.S. Santos, B.F. Nascimento, C.M.B. De Araujo, J.V.F.L. Cavalcanti, F.S. Bruckmann, C.R.B. Rhoden, G.L. Dotto, M.L.S. Oliveira, L.F.O. Silva, M.A. Motta Sobrinho, Removal of chloroquine from the aqueous solution by adsorption onto açaí-based biochars: kinetics, thermodynamics, and phytotoxicity, J. Mol. Liq. 383 (2023) 122162.
[46] L. Sellaoui, L.F.O. Silva, M. Badawi, J. Ali, N. Favarin, G.L. Dotto, A. Erto, Z. Chen, Adsorption of ketoprofen and 2- nitrophenol on activated carbon prepared from winery wastes: a combined experimental and theoretical study, J. Mol. Liq. 333 (2021) 115906.
[47] G.O. Vargas, C. Schnorr, F.B. Nunes, T. Da Rosa Salles, M.Z. Tonel, S.B. Fagan, I. Zanella Da Silva, L.F.O. Silva, S.R. Mortari, G.L. Dotto, C.R.B. Rhoden, Highly furosemide uptake employing magnetic graphene oxide: DFT modeling combined to experimental approach, J. Mol. Liq. 379 (2023) 121652.
[48] C. Yanan, Z. Srour, J. Ali, S. Guo, S. Taamalli, V. Fèvre-Nollet, K. Da Boit Martinello, J. Georgin, S.P.F. Dison, L.F.O. Silva, G.L. Dotto, A. Erto, F. Louis, A. Bakali, L. Sellaoui, Adsorption of paracetamol and ketoprofenon activated charcoal prepared from the residue of the fruit of Butiacapitate: experiments and theoretical interpretations, Chem. Eng. J. 454 (2023) 139943.
[49] I. Ben Khemis, F. Aouaini, S. Knani, A. Ben Lamine, Diclofenac sodium drug adsorption isotherm on carbon xerogels via an advanced two layers model with two energies, Mater. Chem. Phys. 312 (2024) 128620.
[50] A. Ben Lamine, Y. Bouazra, Application of statistical thermodynamics to the olfaction mechanism, Chem. Senses 22 (1997) 67–75.
[51] N. Bouaziz, Y. Ben Torkia, F. Aouaini, A. Nakbi, H. Dhaou, A. Ben Lamine, Statistical physics modeling of hydrogen absorption onto LaNi 4.6 Al 0.4: stereographic and energetic interpretations, Separ. Sci. Technol. 54 (2019) 1–20.
[52] M. Bouzid, N. Bouaziz, Y. Ben Torkia, A. Ben Lamine, Statistical physics modeling of ethanol adsorption onto the phenol resin based adsorbents: stereographic, energetic and thermodynamic investigations, J. Mol. Liq. 283 (2019) 674–687.
[53] S. Knani, M. Khalfaoui, M.A. Hchicha, M. Mathlouthi, A. Ben Lamine, Interpretation of psychophysics response curves using statistical physics, Food Chem. 151 (2014) 487–499.
[54] H.H. Wu, C.W. Chang, D. Lu, K. Maeda, C. Hu, Synergistic effect of hydrochloric acid and phytic acid doping on polyaniline-coupled g-C3N4 nanosheets for photocatalytic Cr(VI) reduction and dye degradation, ACS Appl. Mater. Interfaces 39 (2019) 35702–35712.
[55] A. Yelil Arasi, J. Juliet Latha Jeyakumari, B. Sundaresan, V. Dhanalakshmi, R. Anbarasan, The structural properties of Poly(aniline)—analysis via FTIR spectroscopy, Spectrochim. Acta Mol. Biomol. Spectrosc. 74 (2009) 1229–1234.
[56] M. Ghorbani, H. Eisazadeh, Removal of COD, color, anions and heavy metals from cotton textile wastewater by using polyaniline and polypyrrole nanocomposites coated on rice husk sh, Compos. B Eng. 45 (2013) 1–7.
[57] M. Ghorbani, H. Eisazadeh, Fixed bed column study for Zn, Cu, Fe and Mn removal from wastewater using nanometer size polypyrrole coated on rice husk ash, Synth. Met. 162 (2012) 1429–1433.
[58] A. Yazidi, L. Sellaoui, M. Badawi, G.L. Dotto, A. Bonilla-Petriciolet, A. Ben Lamine, A. Erto, Ternary adsorption of cobalt, nickel and methylene blue on a modified chitin: phenomenological modeling and physical interpretation of the adsorption mechanism, Int. J. Biol. Macromol. 158 (2020) 595–604.
[59] M. Bhaumik, A. Maity, V.V. Srinivasu, M.S. Onyango, Removal of hexavalent chromium from aqueous solution using polypyrrole-polyaniline nanofibers, Chem. Eng. J. 181–182 (2012) 323–333.
[60] M. Bhaumik, S. Agarwal, V.K. Gupta, A. Maity, Enhanced removal of Cr(VI) from aqueous solutions using polypyrrole wrapped oxidized MWCNTs nanocomposites adsorbent, J. Colloid Interface Sci. 470 (2016) 257–267.
[61] Y. Chen, C. Lei, Y.G. Zhao, M.L. Ye, K. Yang, Orientation growth of N-doped and iron-based metal–organic framework and its application for removal of Cr(VI) in wastewater, Molecules 29 (2024) 1007.
[62] R. Soltani, A. Marjani, M. Hosseini, S. Shirazian, Synthesis and characterization of novel N-methylimidazolium-functionalized KCC-1: a highly efficient anion exchanger of hexavalent chromium, Chemosphere 239 (2020) 124735.
[63] E. Hidayat, T. Yoshino, S. Yonemura, Y. Mitoma, H. Harada, A carbonized zeolite/chitosan composite as an adsorbent for copper (II) and chromium (VI) removal from water, Materials 16 (2023) 2532.
[64] S.H. Yu, H. Li, Q.Z. Yao, S.Q. Fu, G.T. Zhou, Microwave-assisted preparation of sepiolite-supported magnetite nanoparticles and their ability to remove low concentrations of Cr(VI), RSC Adv. 5 (2015) 84471–84482.
[65] T. Altun, H. Ecevit, Cr(VI) removal using $Fe_2O_3$-chitosan-cherry kernel shell pyrolytic charcoal composite beads, Environmental Engineering Research 25 (2020) 426–438.
[66] F. Aouaini, S. Knani, M. Ben Yahia, N. Bahloul, A. Ben Lamine, N. Kechaou, Investigation of pore size and energy distributions by statistical physics formalism applied to agriculture products, Physica A 439 (2015) 150–159.
[67] F. Aouaini, S. Knani, M. Ben Yahia, A. Ben Lamine, Statistical physics formalism studies of multilayer adsorption isotherm in food materials and pore size distribution, Physica A 432 (2015) 373–390.
[68] A. Nakbi, M. Bouzid, F. Ayachi, N. Bouaziz, A. Ben Lamine, Quantitative characterization of sucrose taste by statistical physics modeling parameters using an analogy between an experimental physicochemical isotherm of sucrose adsorption on βcyclodextrin and a putative biological sucrose adsorption from sucrose dose-taste response curve (psychophysics and electrophysiology), J. Mol. Liq. 298 (2019) 111950.
[69] A. Nakbi, M. Bouzid, F. Ayachi, F. Aouaini, A. Ben Lamine, Investigation of caffeine taste mechanism through a statistical physics modeling of caffeine dose-taste response curve by a biological putative caffeine adsorption process in electrophysiological response, Prog. Biophys. Mol. Biol. 149 (2019) 70–85.
[70] A. Nakbi, M. Bouzid, I. Ben Khemis, F. Aouaini, A. Ben Hassen, Y. Ben Torkia, A. Ben Lamine, A putative biological adsorption process of binary mixture taste of sucrose and caffeine on human neuroreceptor site by the use of statistical physics modeling, J. Mol. Struct. 1273 (2023) 134225.
[71] B.P. Russell, M.D. LeVan, Pore size distribution of BPL activated carbon determined by different methods, Carbon 32 (1994) 845–855.
[72] B. Diu, C. Guthmann, D. Lederer, B. Roulet, Physique statistique, Hermann, Paris, 1989 (in French).